Available online at www.sciencedirect.com
ScienceDirect
International Journal of Mass Spectrometry 265 (2007) 337–346
International Journal of Mass Spectrometry
www.elsevier.com/locate/ijms

Surface-induced dissociation and reactions of cations and dications $C_7H_8^{\bullet+/2+}$, $C_7H_7^{+/\bullet 2+}$ and $C_7H_6^{2+}$: Dependence of mass spectra of product ions on incident energy of the projectiles

L. Feketeová [a], T. Tepnual [a], V. Grill [a], P. Scheier [a], J. Roithová [b], Z. Herman [a,b,*], T.D. Märk [a]

[a] *Institut für Ionenphysik und Angewandte Physik, Leopold-Franzens Universität Innsbruck, Technikerstr. 25, 6020 Innsbruck, Austria*
[b] *V. Čermák Laboratory, J. Heyrovský Institute of Physical Chemistry, Academy of Sciences, Dolejškova 3, 18223 Prague 8, Czech Republic*

Received 2 November 2006; received in revised form 19 March 2007; accepted 26 March 2007
Available online 30 March 2007

Abstract

Surface-induced dissociation and reactions of singly-charged ions $C_7H_n^+$ ($n = 8$, 7) and of doubly-charged ions $C_7H_n^{2+}$ ($n = 8$, 7, 6), produced by electron ionization of toluene, with hydrocarbon-covered stainless steel surface have been investigated in the incident energy range from 5 to 50 eV. The mass-selected beam of projectile ion was focused onto the surface under 45° and product ions reflected were monitored using a TOF mass spectrometer. The relative abundance of product ions was determined in dependence on incident projectile-ion energy (collision-energy resolved mass spectra, CERMS curves). An important process in surface collisions of the dications is single-electron exchange with the surface and formation of monocation intermediates. Comparison of the mass spectra of the incident cations and dications made it possible to elucidate major reaction pathways.

Keywords: Toluene; Ion-surface collisions; Surface-induced-dissociation

1. Introduction

Studies of collisions of slow ions with surfaces represent a research area that experienced a rapid growth during the past 20 years. Selected physical and chemical processes have been studied by the impact of slow ions of incident energies up to 100 eV [1–6]. These energies and in particular energies transferred during the collision into internal degrees of freedom are of the same order of magnitude or somewhat larger than energies of chemical bonds. Thus, the surface collisions are likely to lead (under consideration of factors that influence dissociation processes, including, e.g., kinetic shifts) to fragmentation of the projectiles (SID, surface-induced dissociations). Studies of such ion-surface interactions can provide useful information on both projectiles and surfaces, ranging from surface diagnostics and surface modification to characterization of projectile ions. In particular, activation of ions in surface collisions and surface-induced dissociation of the projectiles has been successfully used as one of the methods for characterizing structural properties of polyatomic organic or bioorganic ions [3–5]. Surface collisions of multi-protonated bioorganic ions, often produced by electrospray techiques, have been increasingly employed in peptide analysis [7–11]. However, only a few studies exist on a comparison between polyatomic ions of different charges interacting with surfaces [12–19]. They concerned collisions of singly- and doubly-charged ions from toluene ($C_7H_8^{\bullet+/2+}$, $C_7H_7^{+/\bullet 2+}$, $C_7H_6^{2+}$) [12,19], benzene ($C_6H_6^{\bullet+/2+}$) [13–15], fullerene cations and dications [16], and multiply-charged fullerenes C_{60}^{n+}($n = 1$–5) [17–19] with hydrocarbon-covered stainless steel surfaces [12,13,16–18] or surfaces covered with self-assembled monolayers [14–16].

Here we present a comparison of ion-surface interaction of polyatomic cations with their respective dications. The projectile ions are cations and dications formed in electron ionization of toluene, i.e., the ions $C_7H_8^{\bullet+/2+}$, $C_7H_7^{+/\bullet 2+}$, and $C_7H_6^{2+}$. Collisions of these cations and dications from toluene with a stainless-steel surface (presumably hydrocarbon-covered) were investigated earlier at the incident energy of 44 eV by Cooks

* Corresponding author at: V. Čermák Laboratory, J. Heyrovský Institute of Physical Chemistry, Academy of Sciences, Dolejškova 3, 18223 Prague 8, Czech Republic. Tel.: +420 2 6605 3514; fax: +420 2 8658 2307.
E-mail address: zdenek.herman@jh-inst.cas.cz (Z. Herman).

1387-3806/$ – see front matter © 2007 Elsevier B.V. All rights reserved.
doi:10.1016/j.ijms.2007.03.017

and coworkers [12]. Only singly-charged ions were observed as products of surface collisions of these dications. Similar mass spectra for the product ions of both, cations and dications collisions, were interpreted by [12] as an indication that the reaction sequence at the surface for dications was charge transfer followed by unimolecular dissociation. The paper does not mention processes of H-atom transfer from surface material. However, in the mass spectra of unlabeled projectiles at a single, fairly high incident energy these processes would be difficult to discern.

In our recent paper [20] on the interaction of $C_7H_8^{\bullet+/2+}$, $C_7H_7^{+/\bullet 2+}$, and $C_7H_6^{2+}$ projectile ions with a hydrocarbon-covered carbon surface at the incident energy of 25.3 eV (incident angle 30° with respect to the surface), mass spectra, translational energy distributions, and angular distributions of the product ions were measured. In agreement with the conclusions of Cooks and coworkers [12], the primary process in collisions of dications was single-charge exchange at the surface and subsequent dissociation of the monocation, internally excited in the surface interaction. Two mechanisms of formation of the fragment ions were suggested, either via unimolecular decomposition of the inelastically scattered monocation or via fragmentation of a protonated species $(C_7H_8)H^+$ (or $(C_7H_7)H^+$) formed by endoergic hydrogen-atom transfer from the surface hydrocarbons. The translational energy distributions of ions resulting from decomposition of these precursor ions $(C_7H_8)H^+$ (or $(C_7H_7)H^+$) peaked at lower energies than those of ions originating from simple dissociation of the surface-excited scattered ions. The velocity distributions of both inelastically scattered projectile ions and fragment ions had very similar velocity distributions (with regard to the above mentioned different inelasticity of processes of simple dissociation of projectiles and fragmentation of surface-protonated precursors) indicating that the fragmentation occurred after the interaction with the surface in the unimolecular way. Structural considerations were based on available data of the widely studied monocations [21,22] and on recent information on the energetics of the toluene dication [23].

The present paper complements the results of the above mentioned paper [20], where the surface interactions of the projectile ions were studied at single collision energy only. Here, we present data on mass spectra of product ions formed in the interaction of the projectiles with a stainless steel surface, covered at room temperature with hydrocarbons, measured over a wide range of incident energies of the projectiles (5–50 eV). The collision-energy resolved mass spectra (the CERMS curves), obtained in this way, provide information on the dependence of dissociative and reactive processes on incident energy.

The investigation of the incident energy dependence of the surface-induced fragmentation of polyatomic projectile ions provides information on changes of fragmentation with increasing internal energy of the projectile. In surface collisions a fraction of incident energy is transformed into internal excitation of the projectile ion and this fraction was shown to depend linearly on the incident energy in the incident energy range studied in this paper [6,24–26]. For collisions with various surfaces covered with hydrocarbons, the mean value of the incident energy transformed into internal excitation was shown to be about 6% of the incident energy for a variety of projectiles [6,17,24–26]. Despite the fact that the distribution of energy transferred into internal excitation of the polyatomic projectile is rather broad (about 1.5 eV, full width at half maximum [6,24–26]), it provides a possibility to impart to the projectile a defined amount of excitation energy which can be changed in a predictable way. In the case of multiply-charged projectiles, additional internal excitation can come from partial neutralization of the projectile in the surface collision [17].

2. Experimental

The relative abundance of product ions in dependence on incident projectile ion energy (CERMS curves) were measured with the tandem mass spectrometer apparatus BESTOF described in detail in our earlier papers [27,28]. It consists of a double focusing two-sector-field mass spectrometer (reversed geometry) combined with a linear time-of-flight mass spectrometer. Briefly, projectile ions were produced by ionization of toluene with 120 eV electrons in a Nier-type ion source (a commercial CH5 mass spectrometer source), operated normally at pressures of about 2.10^{-5} Torr. The ions formed were extracted from the ion source region and accelerated by 3 kV for mass (and energy) analysis by the double-focusing two-sector-field mass spectrometer. Mass resolution of this selector, higher than $m/\Delta m = 2500$, was sufficient to prepare a projectile ion beam devoid of any ^{13}C admixture. After passing the mass spectrometer exit slit, the ions were refocused by an Einzel lens and decelerated to the required collision energy before interacting with the target surface. Shielding the target area with conical shield plates minimized field penetration effects. The incident impact angle of the projectile ions was kept at 45° and the scattering angle (defined as a deflection from the incident beam direction) was fixed at 91°. The incident energy of ions impacting on the surface is defined by the potential difference between the ion source and the surface for the cations, for the dications it was twice this potential energy difference. A fraction of the product ions formed at the surface exited the shielded chamber through a 1 mm diameter orifice. The ions were then subjected to a pulsed extraction-and-acceleration field that initiated the time-of-flight analysis of the ions. The second mass analyzer was a linear time-of-flight mass selector with a flight tube of about 80 cm length. The mass selected ions were detected by a double-stage channel-plate, connected to a multi-channel scaler (time resolution of 5 ns per channel) and a personal computer. The product ion intensities were obtained by integration of the recorded signals and subtraction of the adjacent ion intensities. The surface was a polished stainless steel surface at room temperature, covered by background hydrocarbons.

3. Results and discussion

Mass spectra (e.g., see Figs. 1 and 2) of product ions from interaction of the projectile ions $C_7H_8^{\bullet+}$, $C_7H_8^{2+}$, $C_7H_7^{+}$, $C_7H_7^{\bullet 2+}$, and $C_7H_6^{2+}$ with a hydrocarbon-covered stainless steel surface in dependence on the incident energy (5–50 eV) are given in Tables 1–3, respectively. Product ion intensities are

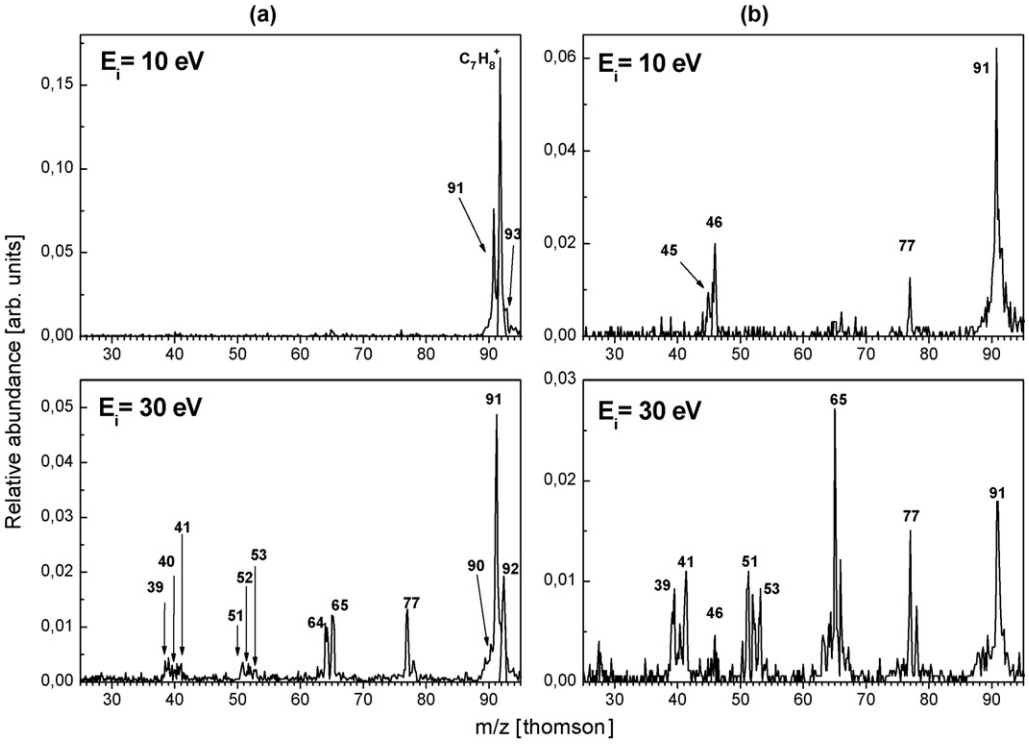

Fig. 1. Mass spectra of product ions from collisions of the projectile ions $C_7H_8^{\bullet+}$ (a) and $C_7H_8^{2+}$ (b) with a hydrocarbon-covered stainless steel surface at incident energies 10 and 30 eV. Incident ion peak hatched.

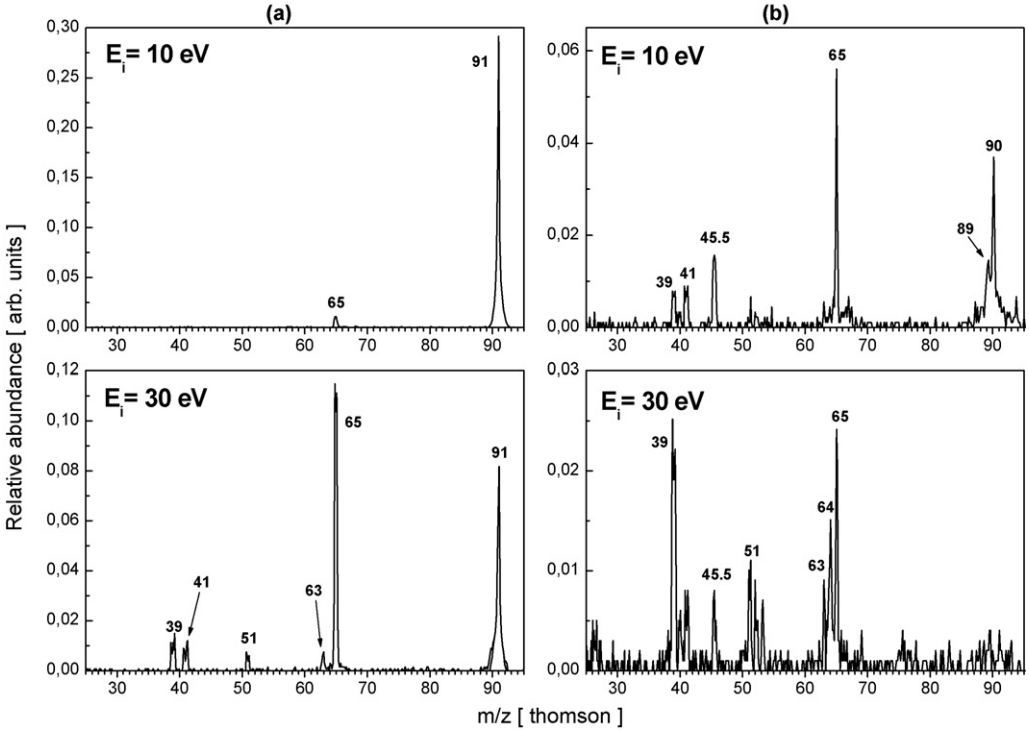

Fig. 2. Mass spectra of product ions from collisions of the projectile ions $C_7H_7^{+}$ (a) and $C_7H_7^{\bullet 2+}$ (b) with a hydrocarbon-covered stainless steel surface at incident energies 10 and 30 eV. Incident ion peak hatched.

Table 1
Mass spectra of product ions from surface collisions of $C_7H_8^+$ and $C_7H_8^{2+}$ in dependece on incident energy (ion abundance in % of total ion abundance, i.e., $I_i/\Sigma I_i$)

m/z	Ion	Incident energy [eV]												
		4	5	7.5	10	12.5	15	20	25	30	35	40	45	50
$C_7H_8^+$														
93	$C_7H_9^+$			8	5.9	10.6	7.6	4.2	5.4	2.3	1.9			
92	*$C_7H_8^+$*	*88.4*	*85.4*	*73.5*	*59.4*	*47.5*	*43.3*	*32*	*16.3*	*12.7*	*6.5*	*4.9*	*2.7*	*1.3*
91	$C_7H_7^+$	11.6	14.6	18.5	29.3	28.6	32.7	46.4	37.6	27	19.3	11.4	10.7	6.6
90	$C_7H_6^+$				3.5	6.4	6.2	1.2	5.9	5.1	5.7	1.9	1	0.8
89	$C_7H_5^+$					2.6	2.8	1.1	5	3.3	2.9			
78	$C_6H_6^+$									2.9	2.8	2.2	2.9	2.5
77	$C_6H_5^+$					0.9	1	4.6	7.3	7.3	8.1	7.3	6.6	3.4
76	$C_6H_4^+$									1	1.3	2	2.2	1.2
65	$C_5H_5^+$				1.9	2.3	4.5	6.7	10	8.5	11	7.9	4.5	4.1
64	$C_5H_4^+$					1.1	2	3.9	7	7.5	12	14.1	10.6	10
63	$C_5H_3^+$								2.8	3.1	2.9	3.3	2.7	3.9
62	$C_5H_2^+$										1.2	2.2	1.6	2.8
53	$C_4H_5^+$									2.1	1.6	3.7	3.2	3.6
52	$C_4H_4^+$									2.2	2.6	4.2	5.5	4.9
51	$C_4H_3^+$								1.1	4	6.7	10.4	11.9	15.7
50	$C_4H_2^+$												1.6	1.4
41	$C_3H_5^+$								1.6	3.5	3.8	5	6.7	6.4
40	$C_3H_4^+$									2.8	3.1	5.5	5.4	6.1
39	$C_3H_3^+$									4.7	5.5	11.1	16	19.3
27	$C_2H_3^+$										1	2.9	4.3	5.9

m/z	Ion	Incident energy [eV]												
		5	6	7.5	9	10	12.5	15	20	25	30	35	40	44	50
$C_7H_8^{2+}$															
93	$C_7H_9^+$		5.7	5.2	3.9	3.1	3								
92	$C_7H_8^+$		11	6.2	14.8	4	4	4.5	3.7	3.1					
91	$C_7H_7^+$		25	34.7	29	43.6	44.5	40.5	33.8	25.2	16.2	8	4.4	4.9	
90	$C_7H_6^+$		8.7	11.4	9.8	4.8									
89	$C_7H_5^+$		4.2	7.8	9.1	6.8	10.8	12.6	8.6	5.5	5.3	3.6	3.4	1.5	
77	$C_6H_5^+$			4.5	5.3	6.2	10.2	9.9	11.9	12.1	5.7	6	4.7		
65	$C_5H_5^+$				3	4	6.2	7.1	6.5	11	11.3	12.3	7.9	9.7	7.5
64	$C_5H_4^+$						1.3	1.7	1.9	3.1	3.6	3.3	4	3	0.7
63	$C_5H_3^+$								0.7	1.2	2.9	2.3	4.5	4	2.2
53	$C_4H_5^+$						1.5	2	4	3.9	4.5	5.8	4.3	3.3	4.3
52	$C_4H_4^+$						2.7	1.7	3.1	4.4	4.5	4.3	5.6	7	3.9
51	$C_4H_3^+$							1.5	2.4	4.7	6.1	5.5	12.3	11.9	15.8
46	*$C_7H_8^{2+}$*	*93.5*	*19.7*	*12.2*	*9.6*	*13.6*	*4.9*	*5.9*	*1.8*	*2.1*	*2.1*	*2.9*			
45	$C_7H_6^{2+}$	6.5	21.6	10.3	6.4	7.1						1.2	2.3	12.2	14
41	$C_3H_5^+$								4	5.4	8.2	7.1	7	8.5	6.5
40	$C_3H_4^+$								2.1	2.5	4.3	5.1	5.3	3.6	5.7
39	$C_3H_3^+$								3.2	4.8	7.8	13.4	14.7	18.2	27.6
27	$C_2H_3^+$									2.2	3	5.6	5.8	7.6	11.1

given as percent fractions of the sum of intensities of all ions measured. The intensities of the projectile ions are given in italics. To make the discussion easier, the CERMS curves of the major product ions are plotted in Figs. 3–7. The lines are polynomial fits through the data points and are only used to guide the eye.

3.1. $C_7H_8^{\bullet+}$ and $C_7H_8^{2+}$

Examples of the recorded spectra of product ions from collisions of the two projectiles, $C_7H_8^{\bullet+}$ and $C_7H_8^{2+}$, are given in Fig. 1a and b for two different incident energies (see also Table 1). The spectra show the presence of the incident projectile ion, the molecular monocation (in case of the dication projectile), and the expected dissociation products. The extent of fragmentation increases with increasing incident energy. In addition, the spectra of both projectiles indicate the presence of ion of *m/z* 93, corresponding to $C_7H_9^+$. In analogy with the previous observation of formation of "protonated projectile ions" in collisions of radical cations with hydrocarbon-covered surfaces [6,19,20,24,25,29,30] we assume that this ion is formed in an analogous chemical reaction of H-atom transfer between hydrocarbons on the surface and incoming projectile ion $C_7H_8^{\bullet+}$ or $C_7H_8^{\bullet+}$ formed after charge exchange of the approaching $C_7H_8^{2+}$. No indication of a chemical reaction of CH_3-addition to the projectile ions, observed earlier in surface collisions of

Table 2
Mass spectra of product ions from surface collisions of $C_7H_7^+$ and $C_7H_7^{2+}$ in dependece on incident energy (ion abundance in % of total ion abundance, i.e., $I_i/\Sigma I_i$)

m/z	Ion	Incident energy [eV]											
		5	7.5	10	12.5	15	20	25	30	35	40	45	50
$C_7H_7^+$													
91	*$C_7H_7^+$*	*98.2*	*96.6*	*95.4*	*92.4*	*85.5*	*66.8*	*44.7*	*34.8*	*20.2*	*9.9*	*4*	*2.6*
66	$C_5H_6^+$						1.2	1.1	1.3				
65	$C_5H_5^+$	1.8	3.4	4.6	7.6	14.5	25.4	39.2	43.4	43.7	40.3	29.1	20.9
64	$C_5H_4^+$									2.3	1.9	2.3	1.9
63	$C_5H_3^+$						1.2	2.1	2.5	4.3	5.7	6.4	7.2
52	$C_4H_4^+$												1.8
51	$C_4H_3^+$						0.9	2.3	3	5.9	8.7	10.1	10.1
50	$C_4H_2^+$											1.7	2.4
41	$C_3H_5^+$						3.2	6	6.7	8.3	8.4	5.3	6.3
39	$C_3H_3^+$						1.3	4.5	8.4	15.3	25.1	39.2	44.1
27	$C_2H_3^+$											2	2.8

m/z	Ion	Incident energy [eV]								
		4	5	7.5	10	12.5	15	20	25	30
$C_7H_7^{2+}$										
91	$C_7H_7^+$	0.8	5.6	8.1	5.6	5.2	4.9	4.3	3.2	
90	$C_7H_6^+$	0.9	32.6	17.2	21.1	12.1	13.2	8	4.3	
89	$C_7H_5^+$		11.8	13.2	11.2	9.3	8.4	7.6		
65	$C_5H_5^+$		16.6	23.8	16.5	28.5	21.3	28.5	19.5	15.3
64	$C_5H_4^+$				2.4	3.2	4.3	5	6.1	10.2
63	$C_5H_3^+$				2.9	4.5	3.8	4.9	7.8	7.1
51	$C_4H_3^+$				2.5	5.7	5.7	3.5	8.5	7.6
45.5	*$C_7H_7^{2+}$*	*98.3*	*20.5*	*17.1*	*10.7*	*12.3*	*8.3*	*5.1*	*6.8*	*5.9*
41	$C_3H_5^+$			5.2	6.3	6.9	8	7.1	5.8	7.8
39	$C_3H_3^+$		7	9	6.1	6.6	12.9	17.3	17.4	25.2

benzene ions [13,14,16] with hydrocarbon-covered surface was observed.

The structure of the projectile ion $C_7H_8^{\bullet+}$ depends on the energy deposited in it during the electron ionization process [22]. Up to about 2 eV of internal excitation the structure of the molecular ion is related to that of the neutral molecule (TOL+), between 2.0 and 2.2 eV the molecular ion can rearrange to the cycloheptatriene (CHT+) structure, above 2.2 eV it begins to fragment. Therefore, the beam of $C_7H_8^{\bullet+}$ projectile ions may be expected to consist mostly of TOL+, possibly with a small amount of CHT+. The ion $C_7H_9^+$ is a product of a chemical reaction of H-atom transfer from surface hydrocarbons. In case of $C_7H_8^{\bullet+}$ collisions with a hydrocarbon-covered surface, formation of $C_7H_9^+$ via this H-atom transfer reaction is endoergic by about 1 eV [20]. Experimental studies of the $C_7H_9^+$ ion produced from toluene [31] indicate that the structure of a major fraction of these ions is related to the σ-complex of the protonated toluene molecule [32], only a minor fraction

Table 3
Mass spectra of product ions from surface collisions of $C_7H_6^{2+}$ in dependece on incident energy (ion abundance in % of total ion abundance, i.e., $I_i/\Sigma I_i$)

m/z	Ion	Incident energy [eV]									
		5	7.5	10	12.5	15	20	25	30	35	40
$C_7H_6^{2+}$											
91	$C_7H_7^+$	5.0	4.3	5.7	8.3	5.7	5.3	4.4	4.2		
90	$C_7H_6^+$	11.5	18.5	18.3	18.2	12.7	11	7	3.8		
89	$C_7H_5^+$	6.5	15.9	15.4	15	12.9	14.1	10.7	7.5		
65	$C_5H_5^+$		6.9	3.4	4.2	7.9	11.7	10.7	8.7	8.5	6.3
64	$C_5H_4^+$		3	5	7.6	9.7	9.8	11.2	10.1	10.2	6.7
63	$C_5H_3^+$		1.8	4	3.6	5.8	7	11.5	14.9	19.1	14.2
62	$C_5H_2^+$				0.9	1.9	3.5	3.6	2.7	5.6	5.2
51	$C_4H_3^+$		1.3	1.5	1.3	2.4	5.3	7.8	7.1	8.4	14.8
50	$C_4H_2^+$					0.9	2.2	1.8	1.7	3.4	3.7
45	*$C_7H_6^{2+}$*	*77.0*	*43.2*	*35.6*	*23.6*	*21.4*	*12.2*	*7.9*	*7.7*	*11.1*	*10.7*
41	$C_3H_5^+$				1.4	1.3	1.9	2	2.5	0	6.8
40	$C_3H_4^+$			1	1.8	2	2.9	2.8	2.9	5.6	4.6
39	$C_3H_3^+$			1.5	2.4	2.8	5.8	9.7	13.4	18.9	21.6

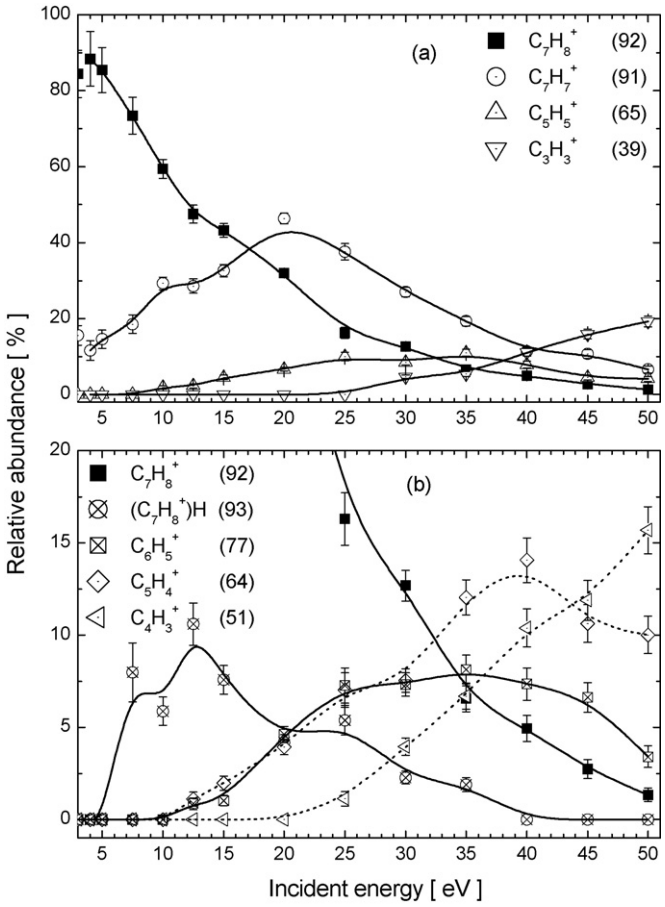

Fig. 3. (a and b) CERMS curves (collision energy resolved mass spectra) for the major product ions from surface collisions of the $C_7H_8^{\bullet+}$ cation. Ion abundance in $I/\Sigma I$, note different ordinate scales.

undergoes a reversible expansion of the ring to protonated 1,3,5-cycloheptatriene. Fragmentation of D- and ^{13}C labeled $C_7H_9^+$ analogues was investigated in detail [33,34] and found to proceed preferentially by H_2 and CH_4 loss. Rearrangements of $C_7H_9^+$were further investigated both experimentally and theoretically [34]. Structures involved in the fragmentation routes have been probed recently by gas-phase infrared spectroscopy of the cation [35].

It follows from the preceding paragraph that the mass spectra of product ions from collisions of $C_7H_8^{\bullet+}$ with a hydrocarbon-covered surface (Table 1) should be discussed taking into account the possibility of fragmentation of both, the surface-collision excited projectile ions $C_7H_8^{\bullet+}$ and the surface-reaction product ions $C_7H_9^+$, formed from the projectile ions by H-atom transfer from hydrocarbons on the surface. The relative abundance of the major product ions from Table 1 is plotted in Fig. 3 in dependence on the incident energy. Fig. 3 shows that the projectile ion $C_7H_8^{\bullet+}$ persists over most of the incident energy range and its abundance gradually decreases. As far as the direct fragmentation of the projectile ion is concerned, the molecular ion $C_7H_8^{\bullet+}$ can easily lose a hydrogen atom and form $C_7H_7^+$. This process can lead in the case of the TOL+ structure directly to the benzyl ion (Bz^+) or via skeletal rearrangements to the tropylium ion (Tr^+). A large amount of experimental and theo-

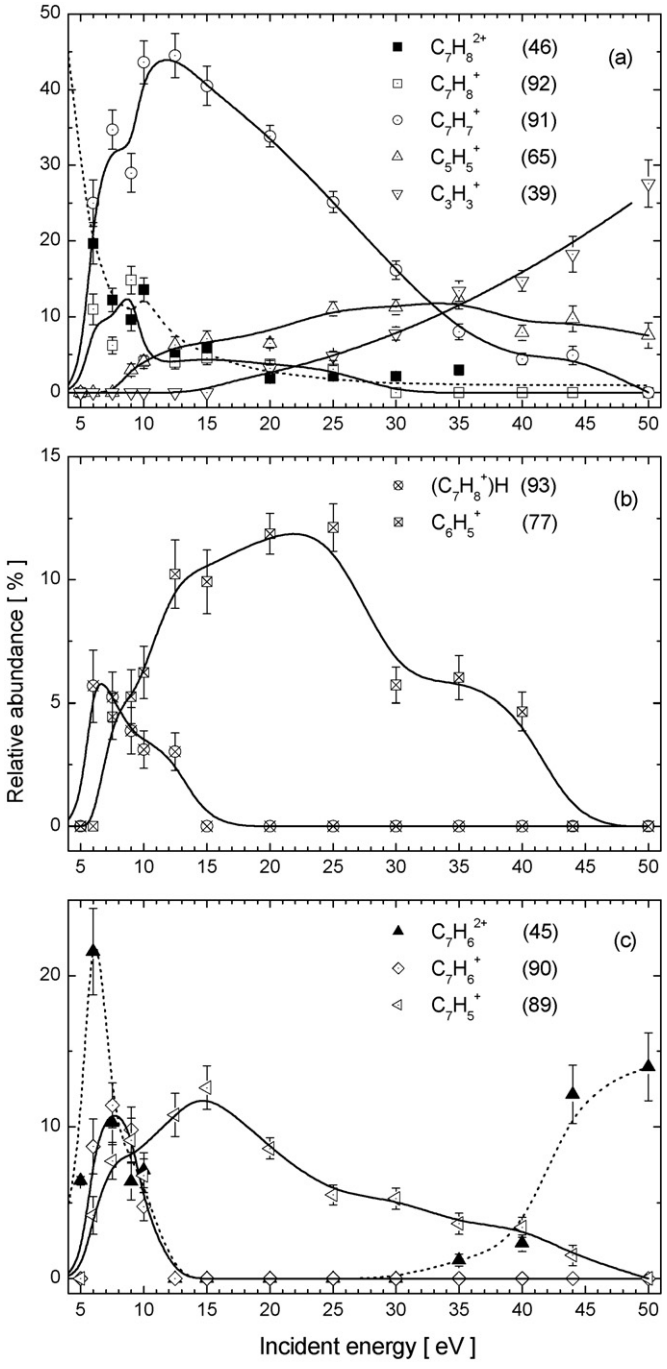

Fig. 4. (a–c) CERMS curves (collision energy resolved mass spectra) for major product ions from surface collisions of the dication $C_7H_8^{2+}$. Ion abundance in $I/\Sigma I$; note different ordinate scales.

retical data dedicated to this problem (see discussion in [21,22]) indicates that the relative populations of the two $C_7H_7^+$ isomers depend on internal energy, formation of Tr^+ being preferred at internal energies of TOL+ below 2 eV [21]. This is presumably our case, as the average internal excitation from surface collisions is about 1.2 eV at the incident energy of 20 eV. The isomer cycloheptatriene cation (CHT+) in the $C_7H_8^{\bullet+}$ beam, if present at all, should decompose by H-atom loss to the Tr^+ ion. Further decomposition of Tr^+ leads in both cases to fragment ions $C_5H_5^+$ and $C_3H_3^+$ by successive elimination of C_2H_2 from

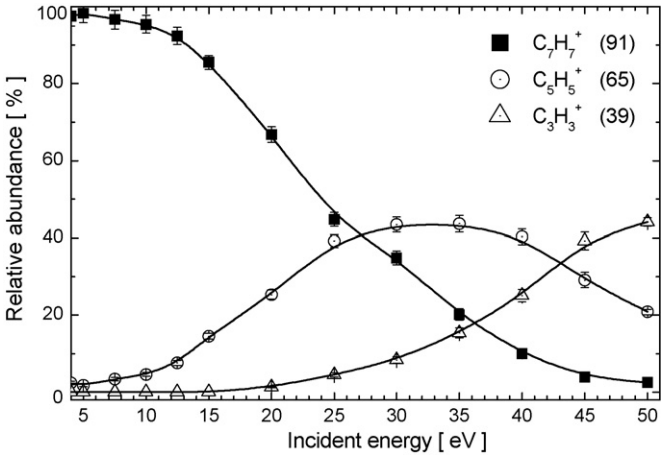

Fig. 5. CERMS curves (collision energy resolved mass spectra) for major product ions from surface collisions of the cation $C_7H_7^+$. Ion abundance in $I/\Sigma I$.

the cyclic structures of these ions. The fragmentation sequence $C_7H_7^+ \rightarrow C_5H_5^+ \rightarrow C_3H_3^+$ can be discerned in the successively increasing abundance of lower mass fragments when going to higher incident energies in the CERMS curves in Fig. 3. The fragment ion $C_7H_7^+$ is formed even at the lowest incident energies, its abundance increases to 40% at about 20 eV and then

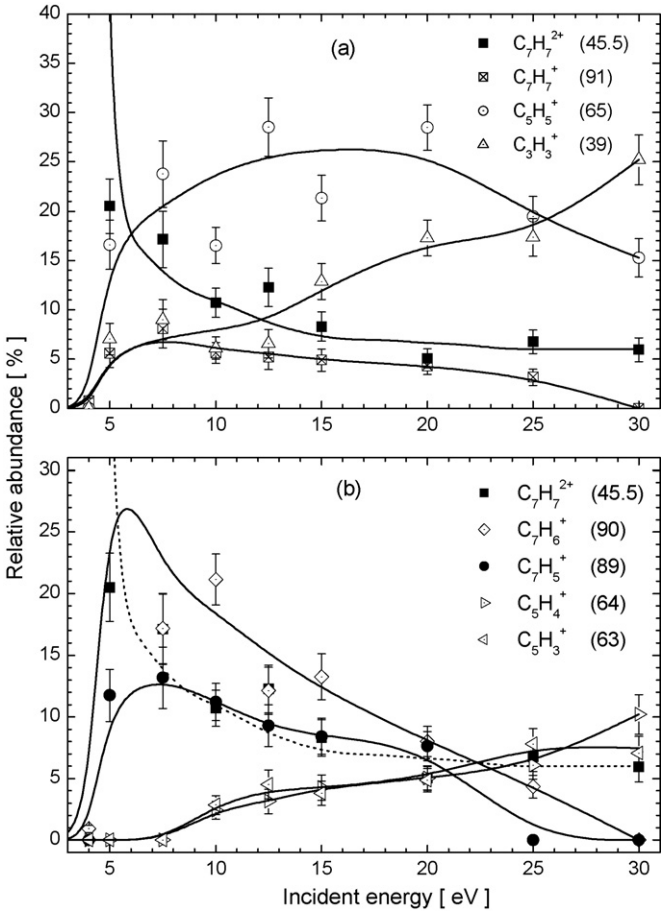

Fig. 6. (a and b) CERMS curves (collision energy resolved mass spectra) for major product ions from surface collisions of the dication $C_7H_7^{\bullet 2+}$. Ion abundance in $I/\Sigma I$; note different ordinate scales.

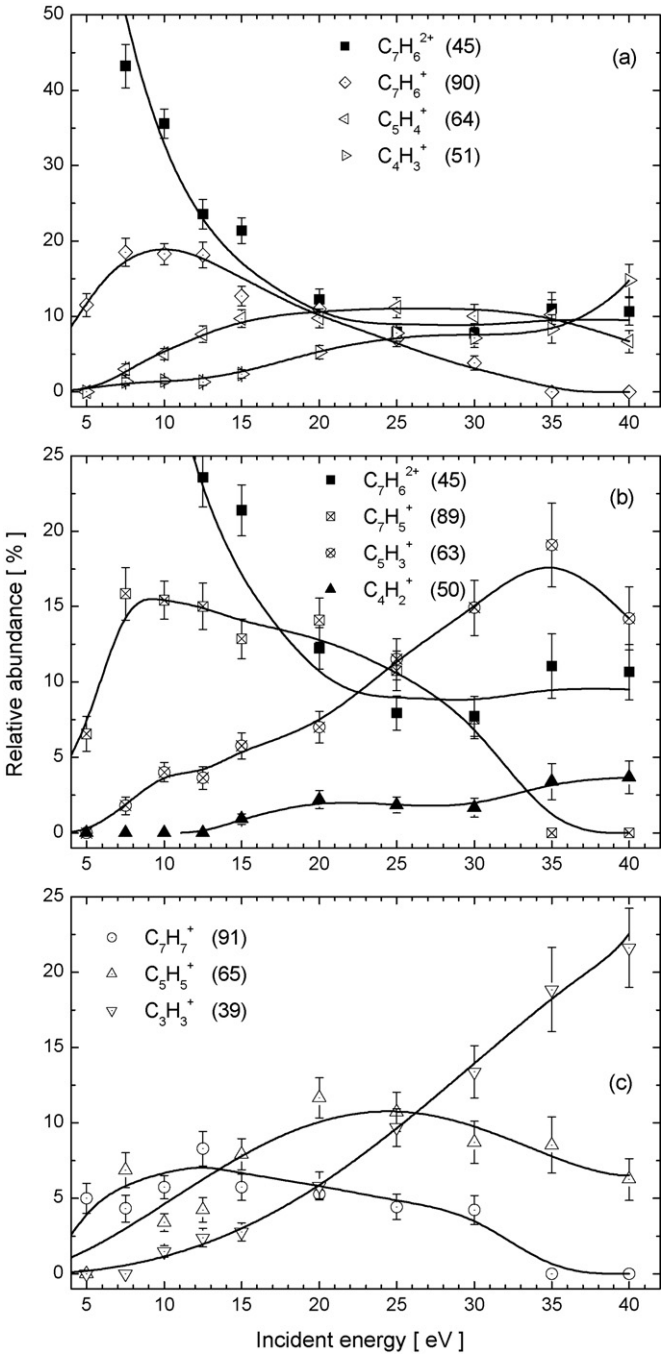

Fig. 7. (a–c) CERMS curves (collision energy resolved mass spectra) for major product ions from surface collisions of the dication $C_7H_6^{2+}$. Ion abundance in $I/\Sigma I$; note different ordinate scales.

gradually decreases, the onset of the ion $C_5H_5^+$ is above 10 eV and the onset of $C_3H_3^+$ above 25 eV, where the abundance of $C_5H_5^+$ starts to decrease.

Surface protonation of the projectile leads to the $C_7H_9^+$ ion; its abundance rises at incident energies above 5 eV. Fragmentation of this ion leads largely to the same products as fragmentation of the projectile ion: elimination of H_2 leads to the formation of $C_7H_7^+$ and elimination of CH_4 to $C_6H_5^+$. Our earlier scattering studies of surface interactions of $C_7D_8^{\bullet +}$ [20] showed that this CH_4 elimination reaction was the major route

for $C_6H_5^+$ formation, while the loss of the CH_3 group from $C_7H_8^{\bullet+}$ was a negligible channel. Translational energy distribution of the product ions showed that $C_7H_9^+$ contributes also to the formation of the $C_5H_5^+$ fragment ions [20]. Further fragment ions of abundance close to 10% are $C_5H_4^{\bullet+}$ and $C_4H_3^+$. Both become more significant at higher incident energies (above 25 eV) and they are most likely produced via further fragmentations of the above mentioned fragment ions.

Recent studies of the $C_7H_8^{2+}$ dication [23] reported that upon electron ionization of toluene most probably a mixture of cycloheptatriene dications and ring-protonated benzylium ions are formed. Electron transfer of these ions at the surface may lead to a variety of structures of the singly-charged $C_7H_8^{\bullet+}$ ions formed. Relative abundances of product ions from surface collisions of $C_7H_8^{2+}$ are given in Table 1 and the CERMS curves of the major product ions are shown in Fig. 4a–c. In contrast to the earlier studies for this ion [12,20] and to studies of other doubly charged ions [13–18], the present results show that the projectile ions survives the surface collision in its dicationic form $C_7H_8^{2+}$, especially at low incident energies. At incident energies 5–10 eV a considerable amount of another dication, $C_7H_6^{2+}$, formed by H_2 elimination from the projectile ion can be observed (Fig. 4c). In this context it is interesting to note that spontaneous dissociation $C_7H_8^{2+} \rightarrow C_7H_6^{2+} + H_2$ was observed as the strongest metastable transition in the fragmentation of $C_7H_8^{2+}$ formed by electron ionization [36]. The dication $C_7H_6^{2+}$ appears as a product ion at incident energies above 30 eV in an amount up to 15%. A possible explanation of this intriguing finding may be found in the recent theoretical and experimental study of the dication and its dehydrogenation [23]. The authors Roithová et al. [23] argue that on the microsecond scale (applicable to the experiments described here) the $C_7H_8^{2+}$ dications from toluene are composed of approximately equal amounts of singlet and triplet states, separated energetically by about 0.09 eV. The triplet state only slowly spin-isomerizes on a longer time scale. The dehydrogenation of the singlet state of $C_7H_8^{2+}$ occurs via ring-protonated and cycloheptatriene structures with an energy barrier of 1.22 eV. However, the triplet state can directly dehydrogenate with a calculated endoergicity of 2.81 eV. The energy difference between the two dehydrogenation processes is thus 1.5 eV.

In our experiments the differences between the threshold of the CERMS curve of $C_7H_6^{2+}$ in Fig. 4c is 30–5 eV = 25 eV. Using the well-know translational-to internal energy conversion on hydrocarbon-covered surfaces of this type of 6% of the incident energy [6,17,24,25], this leads to the difference in activation energies of the two onsets of $C_7H_6^{2+}$ of $0.06 \times 25\,eV = 1.5\,eV$. Therefore, it may be suggested that the low-energy peak (5–13 eV) in the abundance of the product dication $C_7H_6^{2+}$ in Fig. 4c is connected with the dehydrogenation reaction $C_7H_8^{2+} \rightarrow C_7H_6^{2+} + H_2$ of the singlet state of the dication projectile, while in the high-energy region (above 30 eV) the dehydrogenation process involves $C_7H_8^{2+}$ projectile ions in the triplet state. In general, the abundances observed for singly-charged product ions from surface collisions of the dication $C_7H_8^{2+}$ indicate an increased abundance of lower-mass fragments at lower incident energies in comparison with mass spectra of product ions from surface collisions of the monocation $C_7H_8^{\bullet+}$. This suggests a higher internal energy present after charge exchange at the surface, and hence more extensive fragmentation. However, this internal energy gain from the charge transfer process will be considerably smaller than the dication–cation electronic energy difference, in agreement with the results observed earlier in surface collisions of multiply-charged fullerene ions [15,17].

Moreover, in comparison with $C_7H_8^{\bullet+}$ collisions, interactions of the dication $C_7H_8^{2+}$ show an increased abundance of $C_7H_6^{\bullet+}$ and $C_7H_5^+$. These product ions may result from surface interactions of the dication $C_7H_6^{2+}$, formed from the projectile dication in a narrow range of low incident energies (5–10 eV). The charge transfer product cation $C_7H_6^{\bullet+}$ is observed in the same narrow range of incident energies or just above it. The cation $C_7H_6^{\bullet+}$ (practically not observed in electron ionization of toluene) may fragment by H-atom release to $C_7H_5^+$; in addition, the ion $C_7H_5^+$ can be formed by twofold H_2 elimination from $C_7H_9^+$. The fragment ions $C_5H_4^{\bullet+}$ and $C_5H_3^+$ may result from further fragmentation of these two precursors, respectively (see also Section 3.3).

3.2. $C_7H_7^+$ and $C_7H_7^{\bullet 2+}$

The monocation beam of $C_7H_7^+$ should consist mostly of the tropylium ions (Tr^+), with a possible admixture of benzyl ions (Bz^+) [21,22]. Examples of recorded mass spectra are shown in Fig. 2. The mass spectra of product ions are summarized in Table 2 and the CERMS curves of the major ions are given in Fig. 5. The fragmentation of this projectile seems to be the simplest of all ions studied. It fits rather well the fragmentation sequence of the tropylium ion $C_7H_7^+ \rightarrow C_5H_5^+ \rightarrow C_3H_3^+$ involving elimination of C_2H_2 units from the respective cyclic structures. The fragmentation pathway to $C_6H_5^+$ is practically missing. This finding supports our conclusion that in the mass spectra of $C_7H_8^{\bullet+}$ and $C_7H_8^{2+}$ projectile ions, this product ion was formed mostly by CH_4 elimination from $C_7H_9^+$, formed by H-atom transfer reaction at the surface. Translational energy distributions of inelastically scattered undissociated $C_7H_7^+$ and experiments with surface collisions of $C_7D_7^+$ [20] showed that the projectile ion $C_7H_7^+$ can interact with the hydrocarbon-covered surface to produce by H-atom transfer the ion $C_7H_8^{\bullet+}$ in a reaction endoergic by 2–3 eV. Fragmentation of this ion is not specific; it contributes by a small amount to the formation of $C_7H_7^+$ in a reverse reaction and to the formation of $C_5H_5^+$ [20]. However, the contribution of fragmentation of the H-atom transfer product ion $C_7H_8^{\bullet+}$ is rather small and direct fragmentation of the surface-excited projectile ion $C_7H_7^+$ dominates over it [20].

In collisions of the $C_7H_7^{\bullet 2+}$ dications (Table 2 and Fig. 6) again a certain fraction of the doubly charged projectile ions, decreasing with increasing incident energy, survives the surface interaction as dications. However, most of the product ions are singly-charged ions resulting from a single-charge exchange of the dications at the surface. Among the product ions, the fragmentation sequence $C_7H_7^+ \rightarrow C_5H_5^+ \rightarrow C_3H_3^+$ can be clearly seen. However, in comparison with the mass spectra from sur-

face interactions of $C_7H_7^+$ (Table 2, Fig. 5), a higher abundance of fragment ions of lower mass of this sequence occurs at lower incident energies and the onsets of the product ions are shifted to lower energies, too. This indicates again that, due to the internal energy gained in charge exchange, the $C_7H_7^+$ ion thus produced is more internally excited than the respective cation projectile $C_7H_7^+$. In addition, the mass spectra show, in comparison with the mass spectra of product ions from monocation $C_7H_7^+$ collisions, a large abundance of product ions $C_7H_6^{\bullet+}$ and $C_7H_5^+$ and their fragmentation products. This fragmentation sequence is similar to the one in collisions of the $C_7H_6^{2+}$ dication and will be discussed below.

3.3. $C_7H_6^{2+}$

In the case of $C_7H_6^{\bullet+/2+}$ ions, only surface collisions of the dication $C_7H_6^{2+}$ could be investigated, as the respective monocation $C_7H_6^{\bullet+}$ is practically absent in the mass spectra of toluene ionized by electrons. Mass spectra of product ions from surface collisions of the $C_7H_6^{2+}$ dications show that the dications can survive collisions with hydrogen-covered stainless steel surface over the entire incident energy range studied (Table 3 and Fig. 7). Among the singly-charged product ions, $C_7H_6^{\bullet+}$ and $C_7H_5^+$ prevail at low incident energies. The product ion $C_7H_6^{\bullet+}$ results evidently from the charge-transfer reaction of the projectile ion at the surface. Its decomposition products are likely to be $C_5H_4^+$ (elimination of C_2H_2), as the CERMS curve of this ion shows an increase in the vicinity of the incident energy, where the CERMS curve of $C_7H_6^{\bullet+}$ culminates and then decreases (Fig. 7a). At higher collision energies, where the CERMS curve of $C_5H_4^+$ turns down, most probably the elimination of C_3H_3 prevails over the C_2H_2 elimination. The product ion $C_7H_5^+$ is also formed at low incident energy. It presumably results from dissociation of $C_7H_6^{\bullet+}$ by elimination of one hydrogen atom. Also, decomposition of $C_7H_7^+$, formed in H-atom transfer reaction (see below), may contribute to its formation at intermediate incident energies by H_2-elimination. The decomposition products of $C_7H_5^+$ are likely to be $C_5H_3^+$ (C_2H_2 elimination, see increase of the CERMS curve of $C_5H_3^+$ when the CERMS curve of $C_7H_5^+$ decreases after reaching its maximum).

Besides direct decomposition, the radical cation $C_7H_6^{\bullet+}$ formed reacts with the surface hydrocarbons via a H-atom transfer reaction and forms $C_7H_7^+$. Fragmentation of this reaction product gives evidently rise to the dissociation sequence $C_7H_7^+ \rightarrow C_5H_5^+ \rightarrow C_3H_5^+$, as mentioned earlier. Note, however, that the onset of formation of $C_5H_5^+$ and $C_3H_3^+$ is at higher incident energies than in surface collisions of $C_7H_7^{\bullet 2+}$, as if the surface reaction (presumably endoergic) removed some energy from the system.

4. Conclusions

Investigation of the mass spectra of products of surface collisions in dependence on the incident energy may provide useful information on fragmentation channels of surface-excited polyatomic ions even in cases, where information on structure and energetics of the ions is limited. In a surface collision a fraction of the incident energy is transformed into internal energy of the projectile and this fraction increases linearly with increasing incident energy. Though the distribution of the transformed energy is rather broad, surface collisions make it possible to impart to the polyatomic projectile an increasing amount of internal energy. The CERMS curves reflect this increase of the internal energy. The increase and decrease of the relative abundance of product ions with increasing incident energy may thus help in elucidating possible fragmentation sequences.

The present studies of surface collisions of the investigated cations and dications $C_7H_8^{\bullet+}$, $C_7H_8^{2+}$, $C_7H_7^+$, $C_7H_7^{\bullet 2+}$, and $C_7H_6^{2+}$ reveal both similarities and differences. An important process in collisions of dications is evidently single-electron charge transfer of the approaching dication with the surface and formation of singly-charged intermediates that may further decompose. Also, processes of direct fragmentation can be accompanied in some cases by H-atom transfer reactions of the cations with hydrocarbons on the surface and formation of protonated intermediates that may further decompose. The mass spectra observed represent then a mixture resulting from direct dissociation of the projectiles and dissociation of the surface-protonated species.

In all cases, i.e., direct dissociation ($C_7H_8^{\bullet+}$, $C_7H_8^{2+}$, $C_7H_7^+$, $C_7H_7^{\bullet 2+}$) and decomposition of the surface reaction products of $C_7H_6^{2+}$, a major part of the product ion $C_7H_7^+$ fragments in the well-known tropylium decomposition sequence $C_7H_7^+ \rightarrow C_5H_5^+ \rightarrow C_3H_3^+$. In addition, other decomposition sequences were observed for product ions $C_7H_6^{\bullet+}$ and $C_7H_5^+$ being of different importance for different projectile ions: more important in the case of $C_7H_7^{\bullet 2+}$ and $C_7H_6^{2+}$ collisions, less important in other cases.

Dication product ions, usually the surviving projectiles, in case of $C_7H_8^{2+}$ collisions also the fragment dication $C_7H_6^{2+}$, were observed in all cases of dication collisions with hydrogen-covered stainless-steel surface. Their amount decreased with incident energy and it depended on the composition of the dication: at the incident energy of 20 eV it was 1.8% for $C_7H_8^{2+}$, 5.1% for $C_7H_7^{\bullet 2+}$, and 12.2% for $C_7H_6^{2+}$. In case of $C_7H_8^{2+}$ the existence of two energy regions of abundance of the dication product $C_7H_6^{2+}$ may be connected with dehydrogenation of the dication projectile in the singlet and triplet state in processes of different activation energies.

Acknowledgments

Partial support of this research by the Association EURATOM-ÖAW in cooperation with Association EURATOM.IPP.CR is gratefully acknowledged. The content of the publication is the sole responsibility of its publishers and it does not necessarily represent the views of the EU Commission or its services. Work also partially supported by the FWF, Wien and the EU Commission, Brussels and by grants of the Grant Agency of the Academy of Sciences of the Czech Republic (No. 4040405 and No. KJB4040302).

References

[1] J.W. Rabalais (Ed.), Low Energy Ion-Surface Interaction, J. Wiley, New York, 1994.
[2] H. Niehus, W. Heiland, E. Taglauer, Surf. Sci. 17 (1993) 213.
[3] R.G. Cooks, T. Ast, M.D. Mabud, Int. J. Mass Spectrom. 100 (1990) 209.
[4] V. Grill, J. Shen, C. Evans, R.G. Cooks, Rev. Sci. Instrum. 72 (2001) 3149.
[5] T. Ast, J. Serb, Chem. Soc. 66 (2001) 735.
[6] Z. Herman, J. Am. Soc. Mass Spectrom. 14 (2003) 1360.
[7] R.G. Cooks, J.W. Amy, M.E. Bier, J.C. Schwartz, K.L. Schey, Adv. Mass Spectrom. 11 (1989) 33.
[8] A.R. Dongre, A. Somogyi, V.H. Wysocki, J. Mass Spectrom. 31 (1996) 339.
[9] J.M. Gielbert, C. Gu, A. Somogyi, V.H. Wysocki, P.G. Kistemaker, T.L. Weeding, J. Am. Soc. Mass Spectrom. 10 (1999) 414.
[10] J. Laskin, E. Denisov, J.H. Futrell, J. Am. Chem. Soc. 122 (2000) 9703.
[11] J. Laskin, E. Denisov, J.H. Futrell, J. Phys. Chem. B 105 (2001) 1895.
[12] M.A. Mabud, M.J. Dekrey, R.G. Cooks, T. Ast, Int. J. Mass Spectrom. Ion Processes 69 (1986) 277.
[13] M.J. Hayward, M.A. Mabud, R.G. Cooks, J. Am. Chem. Soc. 110 (1998) 1343.
[14] A. Somogyi, T.A. Kane, V.H. Wysocki, Org. Mass Spectrom. 28 (1993) 283.
[15] J.H. Callahan, A. Somogyi, V.H. Wysocki, Rapid Commun. Mass Spectrom. 7 (1993) 693.
[16] A. Somogyi, T.E. Kane, J.-M. Ding, V.H. Wysocki, J. Am. Chem. Soc. 115 (1993) 5275.
[17] F. Biasioli, T. Fiegele, C. Mair, Z. Herman, O. Echt, F. Aumayr, H.-P. Winter, T.D. Märk, J. Chem. Phys. 113 (2000) 5053.
[18] A. Qayyum, C. Mair, T. Tepnual, W. Schustereder, P. Scheier, T.D. Märk, Nucl. Instrum. Methods 205 (2003) 714.
[19] Z. Herman, Int. J. Mass Spectrom. 233 (2004) 361.
[20] J. Jašík, J. Roithová, J. Žabka, A. Pysanenko, L. Feketeová, I. Ipolyi, T.D. Märk, Z. Herman, Int. J. Mass Spectrom. 249–250 (2006) 162.
[21] C. Lifshitz, Acc. Chem. Res. 27 (1994) 138.
[22] C. Lifshitz, Y. Gotkis, A. Ioffe, J. Laskin, S. Shaik, Int. J. Mass Spectrom. Ion Processes 125 (1993) R7.
[23] J. Roithová, D. Schröder, P. Gruene, T. Weiske, H. Schwarz, J. Phys. Chem. A 110 (2006) 2970.
[24] J. Kubišta, Z. Dolejšek, Z. Herman, Eur. Mass Spectrom. 4 (1998) 311.
[25] J. Žabka, Z. Dolejšek, Z. Herman, J. Phys. Chem. A 106 (2002) 10861.
[26] C. Mair, M. Lezius, Z. Herman, T.D. Märk, J. Chem. Phys. 118 (2003) 7090.
[27] C. Mair, T. Fiegele, F. Biasioli, R. Wörgötter, V. Grill, M. Lezius, T.D. Märk, Plasma Sour. Sci. Technol. 8 (1999) 191.
[28] C. Mair, T. Fiegele, F. Biasioli, Z. Herman, T.D. Märk, J. Chem. Phys. 111 (1999) 2770.
[29] J. Roithová, J. Žabka, Z. Dolejšek, Z. Herman, J. Phys. Chem. B 106 (2002) 8293.
[30] J. Jašík, J. Žabka, L. Feketeová, I. Ipolyi, T.D. Märk, Z. Herman, J. Phys. Chem. A 109 (2005) 10208.
[31] R. Bombach, J.-P. Dannacher, J. Stadelmann, J. Am. Chem. Soc. 105 (1983) 4205.
[32] C.H. DePuy, R. Gareyev, S. Fornarini, Int. J. Mass Spectrom. Ion Processes 161 (1997) 41.
[33] D. Koch, J. Schneider, H.-F. Grützmacher, J. Chem. Soc. Perkin Trans. II (1985) 689.
[34] J.-Y. Salpin, M. Mormann, J. Tortajada, M.-T. Nguyen, D. Kuck, Eur. J. Mass Spectrom. 9 (2003) 361.
[35] D. Schröder, H. Schwarz, P. Milko, J. Roithová, J. Phys. Chem. A 110 (2006) 8346.
[36] S. Feil, O. Echt, K. Gluch, V.G. Hasan, S. Matt-Leubner, T. Tepnual, V. Grill, A. Bacher, P. Scheier, T.D. Märk, Chem. Phys. Lett. 411 (2005) 366.